Acta Geochim (2022) 41(3):393–405
https://doi.org/10.1007/s11631-022-00537-y

ORIGINAL ARTICLE

Organic geochemistry characteristics of Jurassic black shales from the Amdo area, northern Tibet, China

Guiwen Xu[1,2,3] · Lan Chen[3] · Weiguang Zhu[1] · Xuejuan Da[3] · Zhangxiong Zhu[3] · Haisheng Yi[4]

Received: 4 February 2022 / Revised: 4 March 2022 / Accepted: 8 March 2022 / Published online: 20 April 2022

Abstract The Jurassic black shales of the Qiangtang Basin, northern Tibet are known to be amongst the most important source rocks. To date, there is no detailed study on the organic geochemistry of the Bathonian/Callovian coccolith-bearing sediments and their source-rock characteristics. Here, we focus on the black limestones, marls, and shales at the Amdo 114 station section using Rock–Eval pyrolysis and biomarkers for sources, types, and thermal maturity of organic matter and the reconstructed depositional environment. All samples are characterized by (1) relatively high TOC values (0.20–2.56 wt%) and relatively low Tmax values between 428 and 452 °C; (2) short-chain *n*-alkanes with a maximum at C_{14} to C_{18} and Pr/Ph > 1; (3) 31–35 homohopanes and gammacerane with lower abundance; and (4) C_{27}–C_{28}–C_{29} regular steranes with C_{29} being slightly dominant. The organic matter is Type II and thus dominantly derived from phytoplankton, especially algae. Thermal maturity indicators include the Ts/(Ts + Tm), C_{31} 22S/(22S + 2R), C_{29} ααα20S/(20S + 0R), C_{29} ββ/(ββ + αα) and C_{27} Dia/(Dia + Reg), which are regarded as immature to very early mature. Additionally, the high Pr/Ph, Pr/nC_{17}, and Ph/nC_{18} ratios, Pr/Ph *vs* Gammacerane index suggest that these black shales were deposited in unstratified marine waters of normal salinity under dysoxic to weakly reduced conditions.

Keywords Rock–Eval pyrolysis · Biomarkers · Source rocks · Jurassic · Northern Tibet

1 Introduction

The marine Jurassic sedimentary successions of the Qiangtang Basin, northern Tibet (China) are well known for their organic carbon-rich shales, abundant fossil content, and the very complete and expanded sections, especially for the Middle to Upper Jurassic strata (Chen et al. 2003, 2014). These Jurassic sediments have been viewed as important exploration targets by numerous petroleum geologists (Chen et al. 2014; Wu et al. 2016). However, a precise understanding of their stratigraphic age, depositional environment, and prevailing palaeo-environmental conditions has been under debate for several decades. Furthermore, the Jurassic strata that contain poorly preserved ammonites, typically squashed flat, are particularly difficult to date. Nevertheless, two Jurassic sections (Biluo Co and Amdo 114 station) in northern Tibet have proven to be relatively rich in coccoliths (Chen et al. 2003), and have recently been dated to the Middle Jurassic, Bathonian to Callovian (Chen et al. 2016, 2019). However, there has been no detailed focus on the organic geochemistry of these coccolith-bearing samples to document the palaeoenvironmental changes across the Bathonian to Callovian boundary. The Biluo Co section exposes

✉ Lan Chen
cllc-10@163.com

[1] State Key Laboratory of Ore Deposit Geochemistry, Institute of Geochemistry, Chinese Academy of Sciences, 99 West Lincheng Road, Guiyang 550081, China

[2] University of Chinese Academy of Sciences, Beijing 100049, China

[3] Department of Earth Sciences, Chongqing University of Science and Technology, Chongqing 401331, China

[4] Institute of Sedimentary Geology, Chengdu University of Technology, Chengdu 610059, China

organic-rich black shales (also called oil shales in the literature), known to be important petroleum source rocks in this area (Chen et al. 2016, 2017). However, the biomarkers at the Amdo 114 station section are poorly understood and few studies have investigated the calcareous nannofossil-rich samples for organic geochemical data to address the relevant palaeo-environmental evolution.

The aim of this study is thus to discuss the palaeo-environmental changes that occurred across the Bathonian to Callovian boundary at the Amdo 114 station section, Qiangtang Basin (northern Tibet, China) integrating Rock–Eval pyrolysis and biomarkers. Based on the organic-matter characteristics, Rock–Eval pyrolysis, and biomarkers, this study gives further insight into the sources and types of organic matter, its thermal maturity, palaeoenvironmental changes during deposition and helps evaluate the hydrocarbon potential of the Qiangtang Basin, Tibet.

2 Geological setting

The Qiangtang block in northern Tibet is sandwiched between the Jinsha suture zone (JSSZ) in the north and the Bangong-Nujiang suture zone (BNSZ) in the south (Fig. 1) (Zhu et al. 2016; Zhang et al. 2017). The northern Qiangtang block is primarily covered by Upper Triassic–Upper Jurassic intercalated marine siliciclastic rocks and limestones, with Carboniferous–Permian shelf strata exposed at its easternmost margin, whereas the southern Qiangtang block contains Carboniferous–Permian shelf-sea sediments, with Triassic–Jurassic marine rocks exposed at its northern and southern limbs (GSC and CIGMR 2013; Zhang et al. 2017).

The Amdo 114 station section is located in the southern Qaingtang block with well-exposed Jurassic sediments, and many geologists have undertaken fieldwork in this area with a focus on petroleum geology or regional investigations. The lower part of this section is composed of conglomerates, sandstones, and siltstones, whereas the middle part is made up of bioclastic limestones and silty limestones. The upper part of the section is characterized by grey-green siltstones, calcareous fine-grained sandstones, dark grey, medium-thick bedded microcrystalline limestones, medium to thin-bedded marls with bioclastic interbeds, and clay-rich and/or silty limestones (Fig. 4 of Chen et al. 2019). Furthermore, the section has provided some molluscs of the Jurassic age (Chen et al. 2006), including the bivalve genera *Buchia*, *Chlamys*, *Posidonia* (*Bositra*) plus some significant ammonites whose stratigraphical ages have proven controversial. The age range of *Bositra* is fixed as Toarcian to Oxfordian (Jefferies and Minton 1965). Additionally, Chen et al. (2016, 2019) found more samples with calcareous nannofossil and provided new data. The presence, from the base of the section, of *Watznaueria barnesiae* suggests at least a Bathonian age; from sample AD-21-1, *W. barnesiae* becomes abundant and the presence in sample AD-16-5 of *Cyclagelosphaera wiedmannii* suggests at least the latter part of the stage (Mattioli and Erba 1999). Also in this section, the range of *Ansulasphaera helvetica* allows the identification of the NJ12 Zone, which spans the interval from the upper Bathonian to the Callovian (Figs. 4 and 6 of Chen et al. 2019).

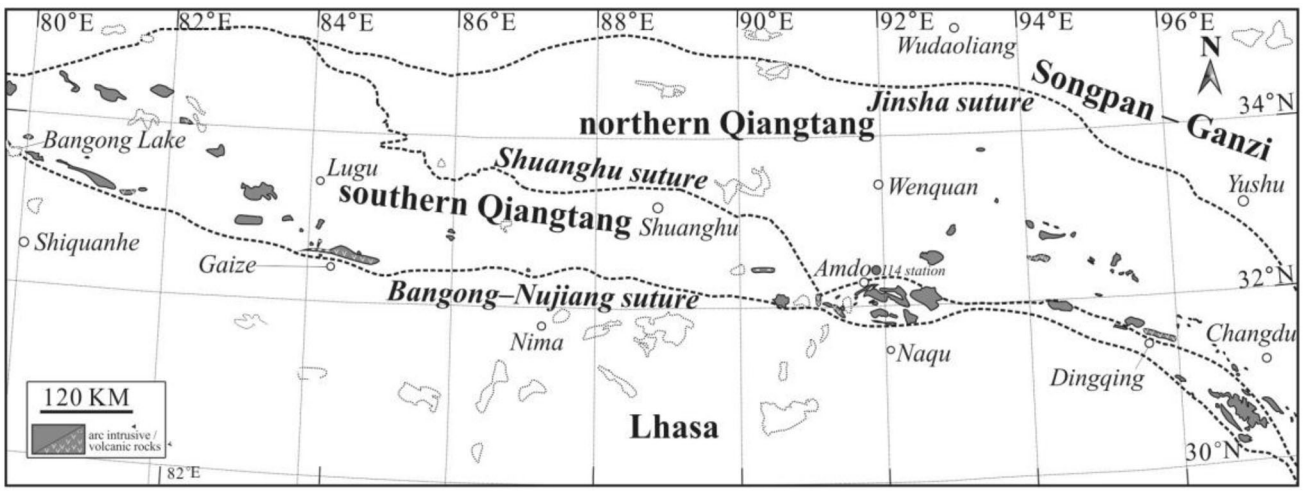

Fig. 1 Simplified tectonic map of the Qiangtang Basin and the studied area (simplified after Zhang et al. 2012, 2017; GSC and CIGMR 2013. Amdo is also spelled as Ando sor Anduo.)

3 Analytical method

3.1 Rock–Eval pyrolysis analyses

Thirteen samples from Amdo 114 station are mainly limestones, marls, and shales. Ten samples contained coccoliths, and 3 samples (AD-5-2, AD-12-1, and AD-34-2) were barren. To obtain information on the type and thermal maturity of the bulk organic matter, Rock–Eval analyses were performed on 13 samples with a Rock–Eval device (Vinci Technologies) under standard conditions (see all details about Rock–Eval pyrolysis and parameters in Espitalié 1993; Behar et al. 2001). Measurements made include S1 (mg HC/g rock), S2 (mg HC/g rock) and Tmax (°C). Derived parameters such as the Total Organic Carbon (TOC) content (wt%), the Hydrogen Index (HI = S2/TOC × 100; mg HC/g TOC) were also determined.

3.2 Biomarkers analyses

Thirteen samples were crushed to 80 mesh and Soxlet-extracted over 72 h with Dichloromethane (DCM) and Methanol (MeOH) (93:7, *v/v*). Total lipid extracts were concentrated and diluted in *n*-hexane for 24 h to precipitate asphaltenes. The other extracts were then separated into three fractions by alumina/silica gel column chromatography using *n*-hexane to elute the saturated hydrocarbons, DCM: *n*-hexane (2:1, *v/v*) for the aromatic hydrocarbons, and DCM: MeOH (93:7, *v/v*) for the polar fraction. The gas chromatography–mass spectrometry (GC–MS) analyses of the saturated fraction were performed on a Shimadzu QP2010plus gas chromatography and an Agilent 5977B mass spectrometer equipped with an HP-5 MS fused silica capillary column (60 m × 0.25 mm inner diameter with a 0.25 μm film coating). The initial GC oven temperature was 50 °C (hold 1 min), and then increased to 120 °C at 20 °C/min, and finally increased to 310 °C at 3 °C/min (hold 25 min). The mass spectrometer was operated in full-scan mode with an electron impact ionization mode at 70 eV. Selective detection of hopanes and steranes was realized by ion extraction (191 and 217, respectively). All experiments were carried out in the National Research Center of Geoanalysis, China.

4 Results

4.1 TOC and Rock–Eval pyrolysis

TOC contents varied between 0.20 and 2.56 wt% (1.06 wt% on average), especially those coccoliths-bearing samples with relatively high TOC contents (> 0.5 wt%) (Table 1). Rock–Eval S1 and S2 contents fall into the ranges of 0.01 and 0.57 mg HC/g rock, and 0.05 and 9.18 mg HC/g rock, respectively. The HI values range from 50 to 394 mg HC/g TOC. Tmax values vary between 428 and 452 °C, with an average of 435 °C. The plot of HI vs Tmax indicates that the organic matter is immature to early mature and has undergone only minor thermal diagenesis (Fig. 2). The organic matter is of Type II.

4.2 Biomarkers

The bitumen contents are relatively low, lying within the range of 0.0205 to 0.1273 % (Table 1), and the extractable hydrocarbons consisted mainly of saturated and polar compounds, with generally high saturate/aromatic ratios (> 1.0, except for three samples with ratios of 0.6 and 0.8; Table 1).

4.2.1 n-Alkanes and isoprenoids

The C_{11}–C_{35} *n*-alkanes are present in the total ion chromatograms (TIC) of the saturated hydrocarbon fractions (Fig. 3), which displays a clear dominance of short-chain (nC_{11}–nC_{19}) relative to long-chain *n*-alkanes (nC_{27}–nC_{35}) with a maximum at nC_{14} to nC_{18}. The values of the carbon preference index (CPI), and odd-to-even predominance (OEP), are in the range of 0.92–1.21 and 0.84–1.13, respectively (Table 1).

All samples have higher concentrations of pristine (Pr) than phytane (Ph) under GC–MS full-scan analyses and strongly varied ratios of the Pr/Ph and isoprenoid/*n*-alkane (Table 1). The Pr/Ph, Pr/nC_{17} and Ph/nC_{18} ratios range from 1.27 to 3.41, 0.60 to 1.13, and 0.31 to 0.51, respectively (Table 1).

4.2.2 Terpanes

The m/z 191 mass chromatogram showed the presence of the C_{27} to C_{35} 17α (H), 21β (H)-hopanes, especially the C_{30}-hopane as the most prominent hopane peak in all samples, while the tri- and tetra-cyclic terpanes are absent (Fig. 4). The C_{27} hopanes are represented by the 17α (H)-22,29,30-trinorhopane (Tm) and the 18α(H)-22,29,30-trinorneohopane (Ts). Furthermore, the pentacyclic terpanes show C_{31} to C_{35} homohopanes, however, from C_{31} homohopane onwards, the homohopanes gradually decrease in abundance, and the C_{33}, C_{34}, or C_{35} homologues occur in low concentrations.

The 22S/(22S + 22R) C_{31} homohopane ratios have reached the equilibrium with values of about 0.6, followed by 0.57–0.66. Furthermore, the Ts/(Ts + Tm) C_{27} hopane diastereomer values fluctuate from 0.16 to 0.46 (except for a value of 0.60 from sample AD-16-2) (Table 2), showing a

Table 1 Basic geochemical data of the Jurassic black rock series at Amdo 114 station section, northern Tibet

Sample no	Lithology	Extractable hydrocarbons (wt %)	Saturates/ aromatics	S_1 (mg/g)	S_2 (mg/g)	Tmax (°C)	TOC (wt %)	HI	RHP	Maximum peak carbon	$\Sigma C_{21}^{-}/\Sigma C_{22}^{+}$	Pr/ Ph	Pr/ nC_{17}	Ph/ C_{18}	CPI	OEP
AD-34–2	Limestone	0.0463	39.0	0.08	0.7	428	0.41	171	1.90	nC_{18}	1.43	1.27	0.76	0.51	0.98	0.95
AD-31–1	Marl	0.1273	1.0	0.46	9.18	429	2.33	394	4.14	nC_{17}	2.98	2.42	1.13	0.49	1.21	1.11
AD-30–2	Shale	0.1100	1.2	0.41	7.79	429	1.99	391	4.12	nC_{16}	1.65	2.03	0.89	0.47	1.03	0.98
AD-28–1	Marl	0.0329	1.4	0.09	0.74	434	0.54	137	1.54	nC_{15}	4.29	2.41	1.09	0.51	1.17	1.07
AD-27–2	Shale	0.0998	0.8	0.57	7.16	427	2.51	285	3.08	nC_{16}	2.98	2.45	0.87	0.47	0.96	0.91
AD-25–1	Marl	0.0388	6.6	0.09	0.8	437	0.57	140	1.56	nC_{17}	1.68	1.99	0.99	0.45	1.12	0.99
AD-23-f1	Marl	0.0574	1.1	0.23	2.7	431	1.24	218	2.36	nC_{16}	2.89	2.17	1.03	0.48	1.05	0.99
AD-22–1	Mudstone	0.0475	0.8	0.16	2.54	437	1.29	197	2.09	nC_{14}	4.23	3.41	1.06	0.35	1.17	1.13
AD-17–1	Shale	0.0298	2.9	0.08	0.52	435	0.49	106	1.22	nC_{14}	2.65	2.20	0.91	0.41	1.08	0.99
AD-16–2	Limestone	0.0235	10.0	0.04	0.14	436	0.19	74	0.95	nC_{16}	7.82	2.16	0.61	0.32	0.98	0.94
AD-15–1	Limestone	0.0205	0.6	0.02	0.11	445	0.16	69	0.81	nC_{17}	2.78	1.47	0.76	0.48	1.14	0.84
AD-12–1	Shale	0.0445	2.5	0.09	0.84	432	0.57	147	1.63	nC_{16}	1.60	1.91	0.60	0.31	0.92	0.86
AD-5–2	Mudstone	0.0275	7.6	0.01	0.05	452	0.1	50	0.60	nC_{16}	3.29	1.89	0.77	0.39	1.13	1.03

HI hydrogen index (mgHC/gTOC), *RHP* relative hydrocarbon potential = (S1 + S2)/TOC (mgHC/gTOC), *CPI* carbon preference index = $((C_{23} + C_{25} + C_{27} + C_{29})/(C_{22} + C_{24} + C_{26} + C_{28}) + (C_{23} + C_{25} + C_{27} + C_{39})/(C_{24} + C_{26} + C_{28} + C_{30}))/2$ (Bray and Evans 1961), *OEP* odd or even preference = $(C_{21} + 6C_{23} + C_{25})/(4C_{22} + 4C_{24})$ (Scalan and Smith 1970)

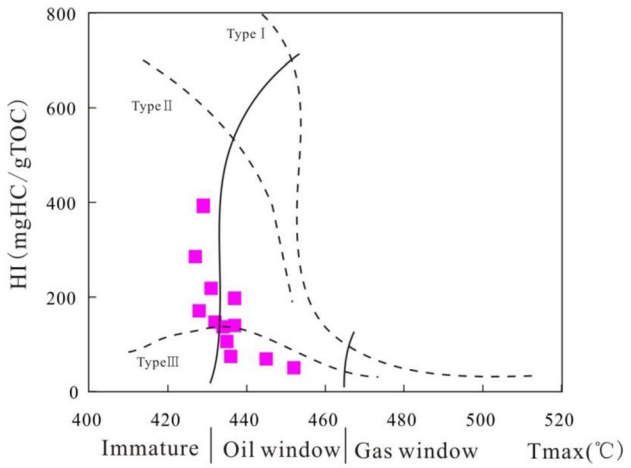

Fig. 2 The plot of HI (mgHC/gTOC) VS. Tmax (°C) indicates that the organic matter is immature to oil window. The boundary lines that denote the different kerogen types are referred to Espitalié et al. (1986)

higher abundance of the thermally less stable trisnorhopane (Tm) than trisnorneohopane (Ts). This pattern corresponds to relatively low thermal maturity levels. Additionally, gammacerane identified in the m/z 191 chromatograms (Fig. 4) shows very low concentrations and the gammacerane/(gammacerane + $\alpha\beta C_{30}$ hopane) index (Sinninghé-Damsté et al. 1995) ranges from 0.01 to 0.06 (Table 2).

4.2.3 Steranes

According to the m/z 217 mass chromatogram (Fig. 5), the C_{27} to C_{29} regular steranes are predominant, the rearranged C_{27}–C_{29} diaster-13(17)-enes are present, but the C_{21} and C_{22} pregnanes are lacking. Distribution of the C_{27} to C_{29} regular steranes indicated an only slight preference for either C_{27} or C_{29} steranes, which is similar to the Ediacaran-Lower Cambrian source rocks from the Sichuan Basin (South China) (Cheng et al. 2018), but is significantly different from Jurassic samples of the Yanshiping area (Northern Tibet) (Chen et al. 2014). The ratios C_{29} $\alpha\alpha\alpha$ 20S/(20S + 20R) vary between 0.35 and 0.47 (Table 2), which is below the thermal equilibrium of 0.52–0.55 at about a value of 0.8 for vitrinite reflectance (Peters et al. 2005). The C_{29} $\beta\beta/(\alpha\alpha + \beta\beta)$ ratios have relatively stable values of about 0.27–0.41, and the C_{27} diasteranes/(diasteranes + regular steranes) ratios of 0.38–0.48 (Table 2).

5 Discussion

Generally speaking, biomarkers can be used to discuss sources, types, and maturities of organic matters, even certain environments of sedimentary rocks, especially organic-carbon-rich black shales (Peters et al. 2005; Song et al. 2017; Aderoju and Bend 2018; Xu et al. 2019).

5.1 Sources of organic matter

Based on the *n*-alkane distributions, it can be distinguished the origin of the organic matter in terms of terrestrial versus marine (Quijano et al. 2012). All studied samples from Amdo 114 station are characterized by short-chain *n*-alkanes ($< nC_{20}$), which indicates algal, phytoplankton, and bacteria sources. However, the medium-chain *n*-alkanes (nC_{21}–nC_{25}) also occurred (Fig. 3), which originate from vascular plants, microalgae, cyanobacteria, *Sphagnum* spp., and aquatic macrophytes (Bingham et al. 2010). In addition, Table 1 shows the CPI and OEP values of 0.92 to 1.21 and 0.84 to 1.13, respectively.

The hopanoids have been widely proposed to derive from the bacteriohopanetertrol and 3-desoxyhopanes, which are present in prokaryotic organisms (i.e. bacteria) and fungi (Bechtel et al. 2001). Summons et al. (1999) suggested that the C_{30} to C_{35} homologues with 22S/R-isomers of 17α(H), 21(β)-homohopanes are sourced by cyanobacteria. Fig. 4 indicates a series of 17α(H), 21(β)-homohopanes (C_{27}–C_{29} tricyclic terpanes and C_{30}–C_{35} hopanes) with relatively high abundances in all samples, which indicate significant bacterial input to the sources of organic matter. However, gammacerane is in very low abundance in these samples. Although it is not a bacterial compound, gammacerane typically occurs when bacteria are present in the water column (Sinninghé-Damsté et al. 1995; Rashby et al. 2007).

By comparison, steranes are formed from precursor sterols, which are detected in all eukaryotes (i.e. algae, higher plants) but rarely in prokaryotes (Bechtel et al. 2001). The relative abundances of C_{27}, C_{28}, and C_{29} steranes are shown in Table 2 and plotted in Fig. 6, but 9 samples are lacking C_{28} regular steranes. All samples are characterized by lower C_{27}/C_{29} ratios from 0.47 to 0.81, and the C_{28}/C_{29} ratios of 4 samples are < 0.36. The distribution of C_{27}–C_{28}–C_{29} regular steranes are shown in a ternary plot with C_{29} always being dominant (47.3–65.6 %), C_{27} intermediate (29.5–44.7 %), and C_{28} minor (16.1–19.6 %) (Fig. 6). The relative distributions of C_{27}–C_{28}–C_{29} regular steranes are similar, but considerable variability within that proportionality is present. Moreover, the data points suggested that the steranes were mainly derived from terrestrial plants. However, the C_{29} steranes

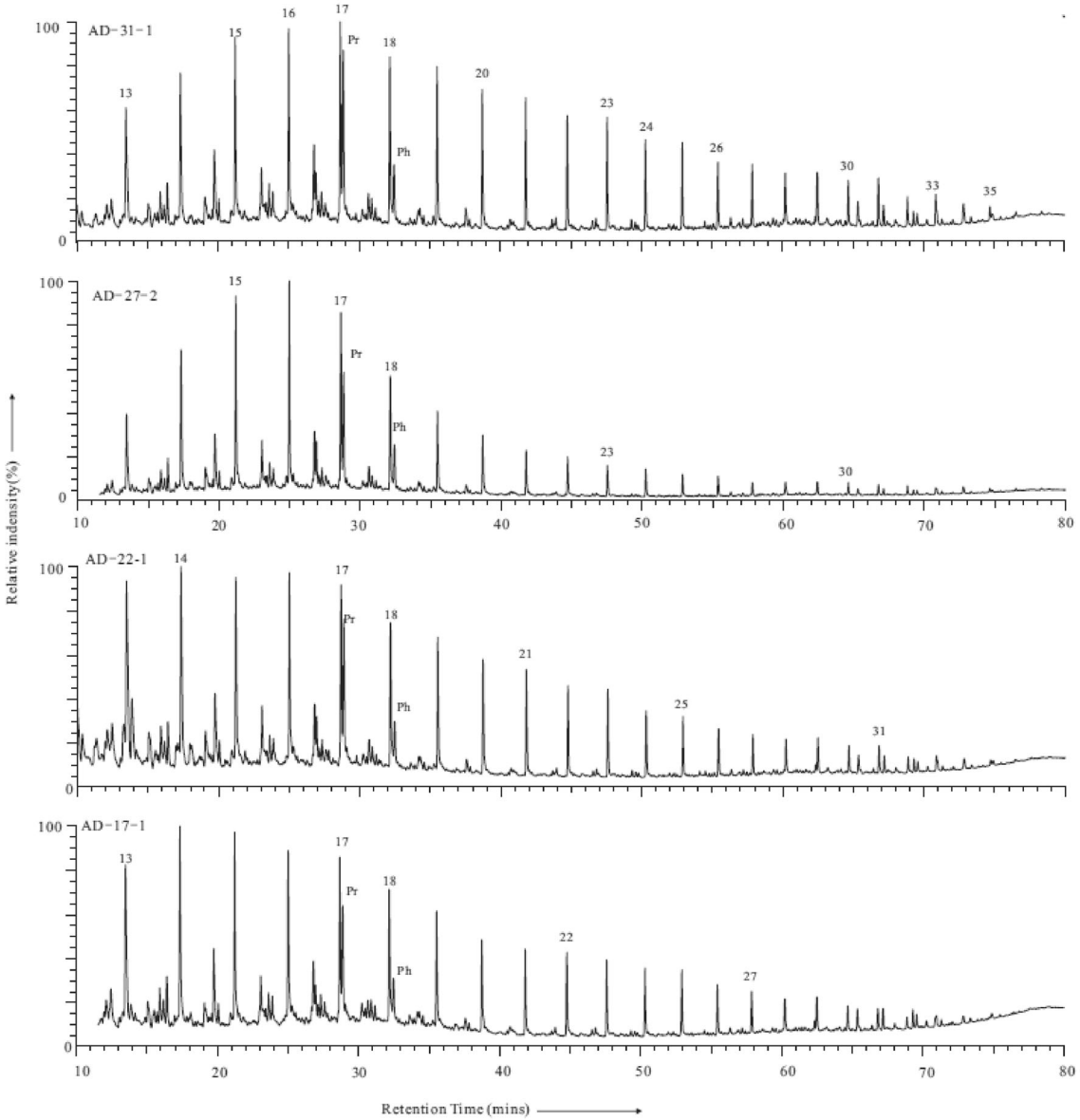

Fig. 3 Total ion Chromatograms (TICs) of the selected samples from Amdo 114 station, Qiangtang Basin (Tibet, China). Numbers above symbols denote carbon numbers

could also come from microalgae. Therefore, our studied samples indicate a relatively high contribution of phytoplankton, especially algae, as the primary source.

Importantly, the nannoflora indicate an increase in trophic level in the higher part of the sections, being a similar phenomenon to that observed in Callovian–Oxfordian Tethyan strata and implying a regional if not a global palaeoceanographic phenomenon that locally-led to the deposition of organic-rich black shales (Chen et al. 2019).

5.2 Thermal maturity trends

Biomarkers, as indicators of the thermal history of organic matter, can be used and have been applied to source rocks, oils (including tars, biodegraded oils, etc.), and even to fluids produced from very young sediments affected by hydrothermal activity (Peters et al. 2005; Blumenberg et al. 2012; Sachse et al. 2012). Molecular indicators of thermal maturity by sterane isomerization generally include the C_{29} ααα20S/(20S + 20R), C_{29} ββ/(ββ + αα) and C_{27} Dia/(Dia + Reg). A cross-plot of C_{29} ααα20S/(20S + 20R) *vs* C_{29} ββ/(ββ + αα) sterane ratios is particularly effective in assessing thermal maturity (Fig. 7a; Peters et al. 2005). In

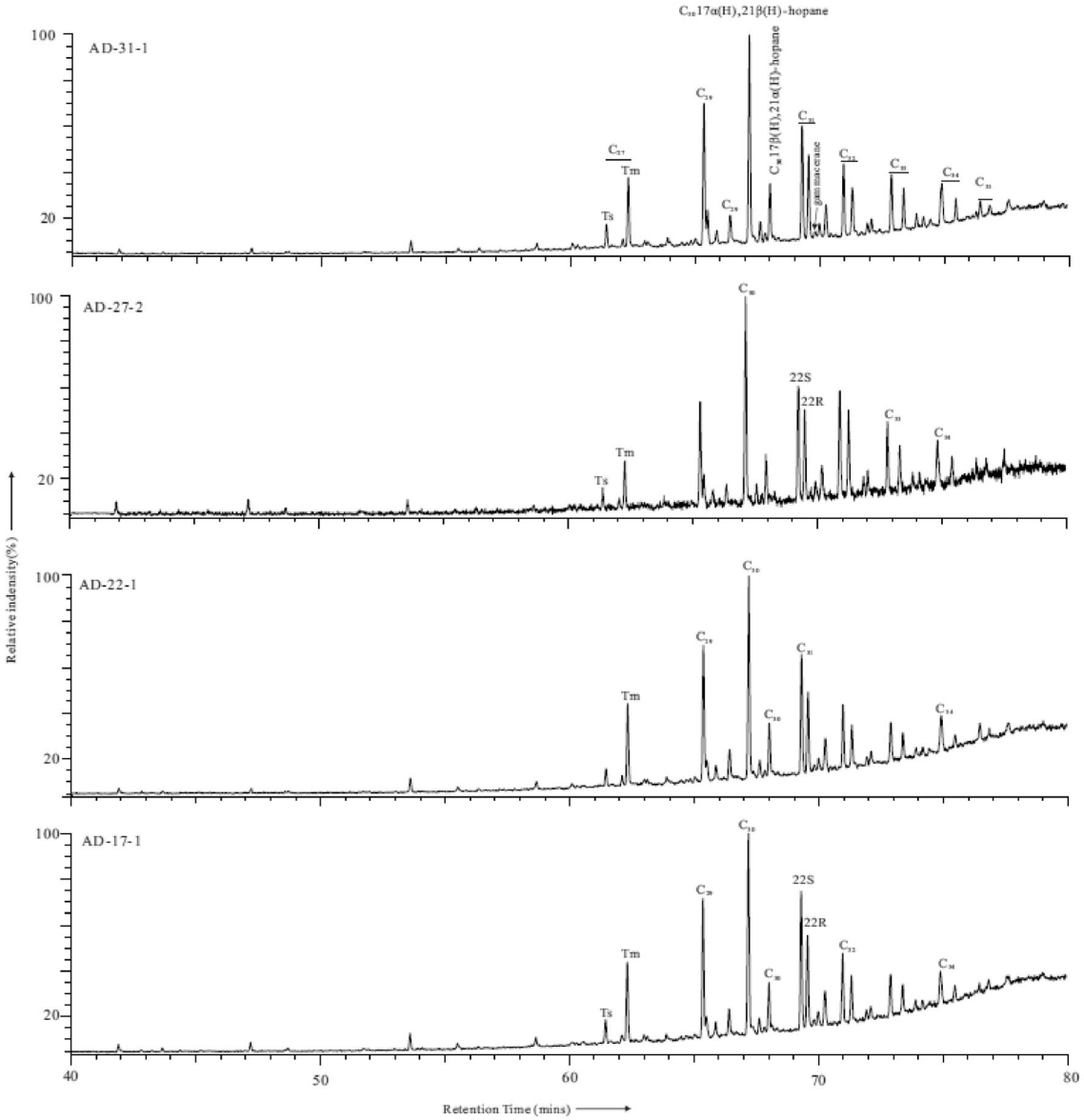

Fig. 4 The *m/z* 191 chromatograms showing relative abundance of terpenoids in the selected samples. Ts, 18α(H)-22,29,30-trisnorneohopane; Tm, 17α(H)-22,29,30-trisnorneohopane. The 22S and 22R epimers are shown for C_{31}-homohopanes

general, the equilibrium at a value of ca. 0.55 of the C_{29} ααα20S/(20S + 20R) ratios corresponds to about 0.8% VRr. In addition, the C_{29} ββ/(ββ + αα) ratios increase with thermal maturity to ∼ 0.7 (0.67–0.71 = equilibrium) at about 0.9% VRr (Peters et al., 2005). In the studied section, steranes are characterized by ββ/(ββ + αα) ratios between 0.27 and 0.41, 20S/(20S + 20R) between 0.35 and 0.47, and C_{27} Dia/(Dia + Reg) between 0.38 and 0.48, respectively (Table 2 and Fig. 7). These values, rather invariable and far away from the equilibrium area, are regarded as immature to very early mature indicators for petroleum generation.

Transformation of the biologically produced 22R form of the C_{31}–C_{35} extended 17α(H)-hopanes to the 22S epimer is illustrated in Fig. 0.4. The m/z 191 mass chromatograms show the changes in proportions of C-22 epimers with increasing maturity. At equilibrium, the approximate proportions are 55–60 % 22S and 40–45 % 22R (Waples and Machihara, 1991). Therefore, the ratios of 22S/(22S + 22R) homohopane are also regarded as maturity indicators. The studied samples showed ratios of 22S/(22S + 22R) from 0.57 to 0.66, close to the equilibrium, whereas high values can also occur in hypersaline depositional environments (ten Haven et al. 1987). With increasing maturity, the 17α-22,29,30-trisnorneohopane (Tm) gradually disappears and the 18α-22,29,30-trisnorneohopane (Ts) increases in relative concentration. In practice, however, Ts/(Ts + Tm) ratios should be

Table 2 The hopanes and steranes ratios of the Jurassic black rock series from Amdo 114 station, northern Tibet

Sample no	Lithology	Hopanes					Steranes						
		C_{27}Ts/ (Ts + Tm)	C_{31}22S/ (22S + 22R)	C_{30}M/ (H + M)	Gamm/ (Gamm. + C_{30}Hop.)	C30βα/ (βα + αβ)	ααα 20R regular sterane (%)			C_{27}/ C_{29}	C_{29}αββ/ (αββ + ααα)	C_{29}20S/ (20S + 20R)	C_{27}dia/ (dia + reg)
							C_{27}	C_{28}	C_{29}				
AD-34–2	Limestone	0.33	0.58	0.18	0.06	0.18	35	–	65	0.54	0.32	0.37	0.42
AD-31–1	Marl	0.24	0.58	0.22	0.02	0.22	34	17	49	0.70	0.30	0.35	0.41
AD-30–2	Shale	0.23	0.59	0.20	0.03	0.20	45	–	55	0.81	0.33	0.41	0.48
AD-28–1	Marl	0.27	0.58	0.18	0.05	0.18	34	–	66	0.52	0.35	0.36	0.46
AD-27–2	Shale	0.30	0.62	0.16	0.02	0.16	40	–	60	0.65	0.35	0.36	0.41
AD-25–1	Marl	0.32	0.59	0.20	–	0.20	30	17	53	0.57	0.27	0.40	0.40
AD-23-f1	Marl	0.24	0.59	0.17	0.01	0.17	30	20	51	0.58	0.31	0.39	0.44
AD-22–1	Mudstone	0.16	0.58	0.23	0.02	0.23	37	16	47	0.77	0.35	0.41	0.40
AD-17–1	Shale	0.21	0.59	0.20	0.03	0.20	38		62	0.63		0.42	0.38
AD-16–2	Limestone	0.60	0.61	–	–	–	–	–	–	–	–	–	–
AD-15–1	Limestone	0.46	0.66	–	–	0.13			–	–	–	–	–
AD-12–1	Shale	0.38	0.57	0.16	0.04	0.16	33	–	67	0.50	0.41	0.36	0.45
AD-5–2	Mudstone	0.27	0.59	–	–	0.18	32	–	68	0.47	0.35	0.47	–

Gamm Gammacerane, *Hop*. Hopane, *M*. Moretane, *Dia.* Diasterane, *Reg.* Regular sterane, – no data

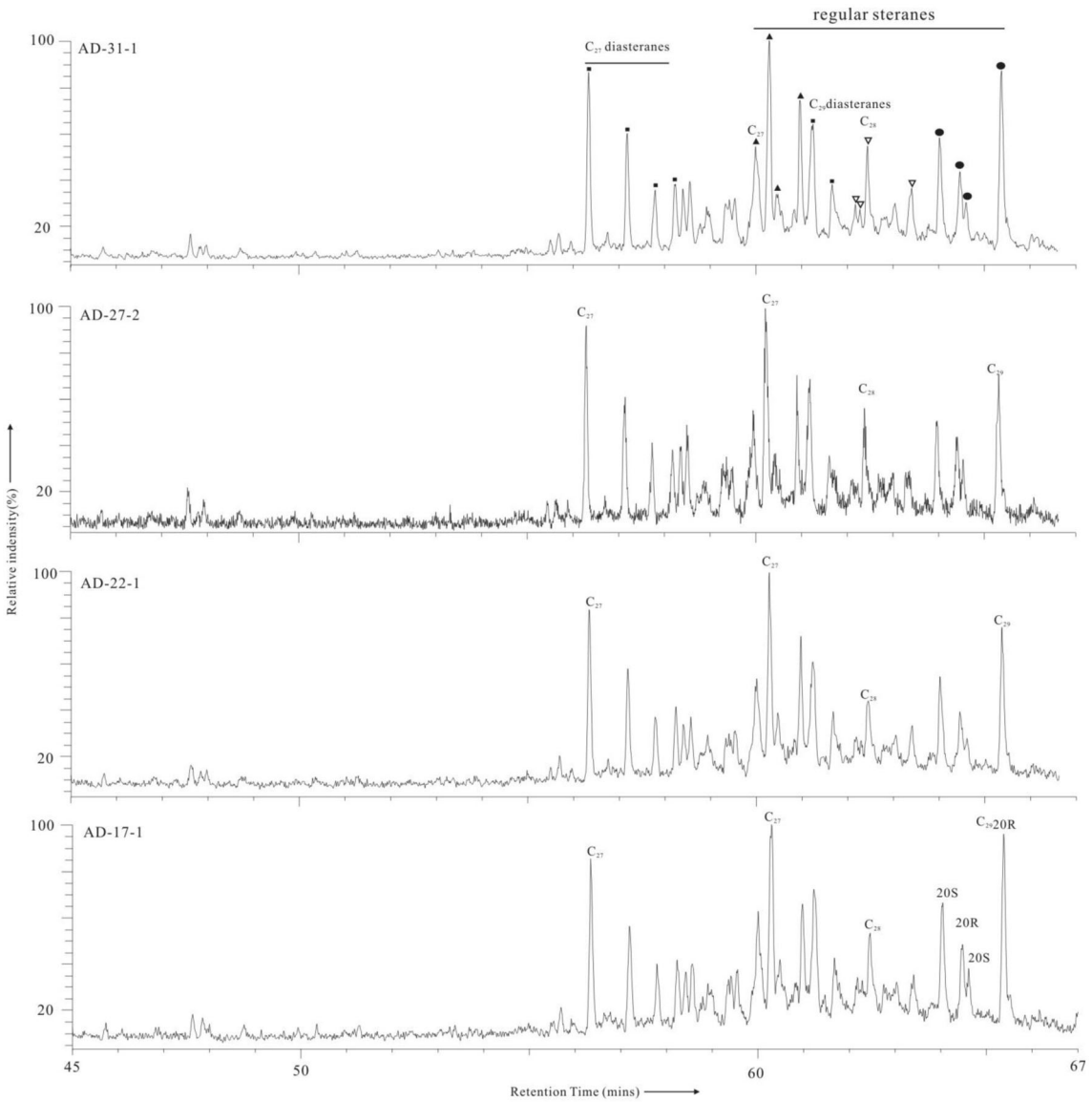

Fig. 5 The *m/z* 217 chromatograms showing relative abundance of steriods in the selected samples. The 20S and 20R epimers are shown for C_{29} regular steranes

influenced by facies, salinity, and redox conditions as well as maturity (Peters et al. 2005). All samples from Amdo 114 station show lower Ts/(Ts + m) ratios from 0.16 to 0.60. Additionally, Tmax values change between 427 and 452 °C, and the plot of HI/Tmax indicates that the OM is immature to the oil window (Fig. 2). The above-shown data indicate that the Middle Jurassic sediments from Amdo 114 station section are immature to early mature concerning oil generation. This interpretation is also consistent with those parameters shown in Fig. 8.

5.3 Redox conditions

The Pr/Ph ratio has been used to infer depositional redox conditions but is also influenced by several other factors (e.g. thermal maturity, variable biomolecule sources, lithology, and diagenetic effects) (Peters et al. 2005). In general, the high Pr/Ph ratios (> 1.27) indicate oxidizing depositional conditions (> 0.8; Hughes et al. 1995). Fig. 8 showed the high Pr/nC_{17} and Ph/nC_{18} ratios, however, all samples are characterized by dark colors, lamination, and calcareous nannofossils. Therefore, all samples indicated dysoxic to weakly reduced bottom waters.

In addition, high ratios of C_{30} moretane/(moretane + hopane), 22S/(22S + 22R)C_{31} homohopane and

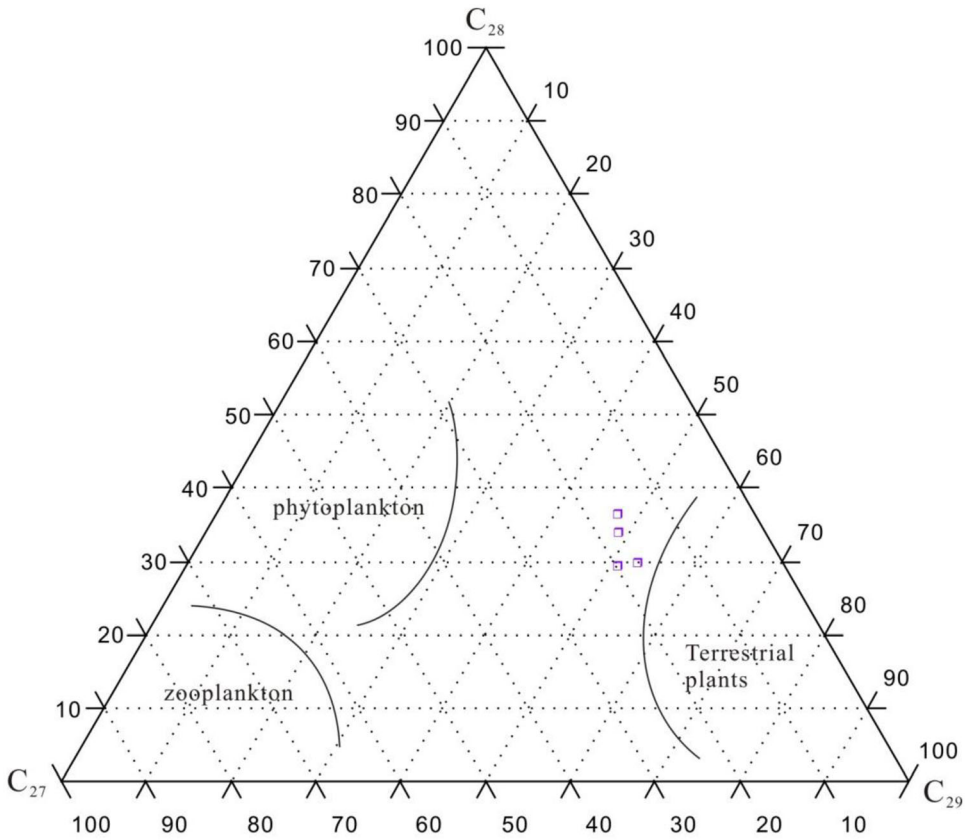

Fig. 6 Relative composition of C_{27}, C_{28} and C_{29} steranes from the studied samples showing the organic matter stems mainly from phytoplankton

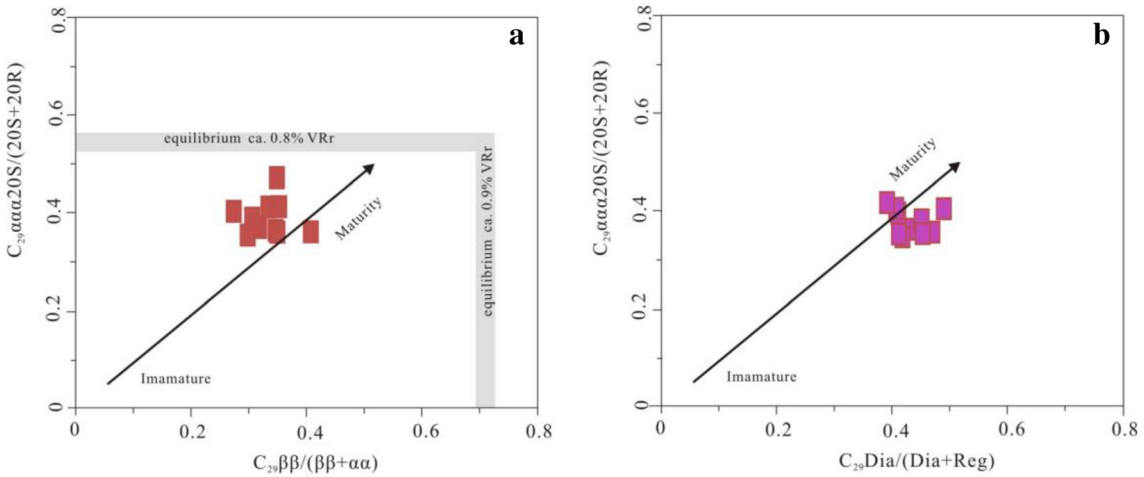

Fig. 7 Maturity-related biomarker parameters by sterane isomerization. **a** C_{29} ααα 20S/(20S + 20R) vs. C_{29} ββ/(ββ + αα). **b** C_{29} ααα 20S/(20S + 20R) vs. C_{27} diasterane/(diasterane + regular sterane)

Ts/(Ts + Tm), as well as high gammacerane contents and gammacerane index [gammacerane/(gammacerane + C_{30}-Hopane)], are considered to be markers for the enhanced water salinity and water-column stratification (commonly resulting from hypersalinity at depth) (Sinninghe Damsté et al. 1995; Peters et al. 2005; Song et al. 2017; Aderoju and Bend 2018). All samples from Amdo 114 station section are characterized by gammacerane with low abundance (Fig. 4), a gammacerane index with low values in the range of 0.02–0.10 (Table 2), and Ts/(Ts + Tm) ratios between 0.16 and 0.46 (except for 0.60 of sample AD-16-2) (Fig. 9a, d), but the C_{30} Moretane/(Moretane + Hopane) and Pr/Ph with high ratios (Fig. 9b, c). Together, these organic geochemical data suggest normal marine salinity, redox conditions varying from dysoxic to weakly reduced, and an absence of water-column

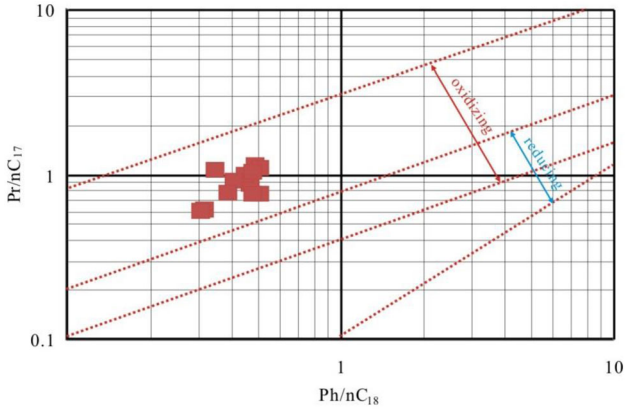

Fig. 8 Pr/nC_{17} vs. Ph/nC plot for all samples indicating deposition under oxidizing to oxygen-depleted conditions. The reference lines are from Didyck et al. (1978)

stratification during deposition of the Middle Jurassic black shales in Tibet.

6 Conclusions

All samples containing abundant organic matter from Amdo 114 station, northern Tibet were investigated for Rock–Eval pyrolysis and biomarker compositions. Those samples with abundant coccoliths and relatively elevated TOC, dated as Bathonian/Callovian, are shown to have organic matter derived mainly from phytoplankton or algae. Redox conditions in the depositional environment varied from dysoxic to weakly reduced, salinity was normal, and there is no evidence for a stratified water column.

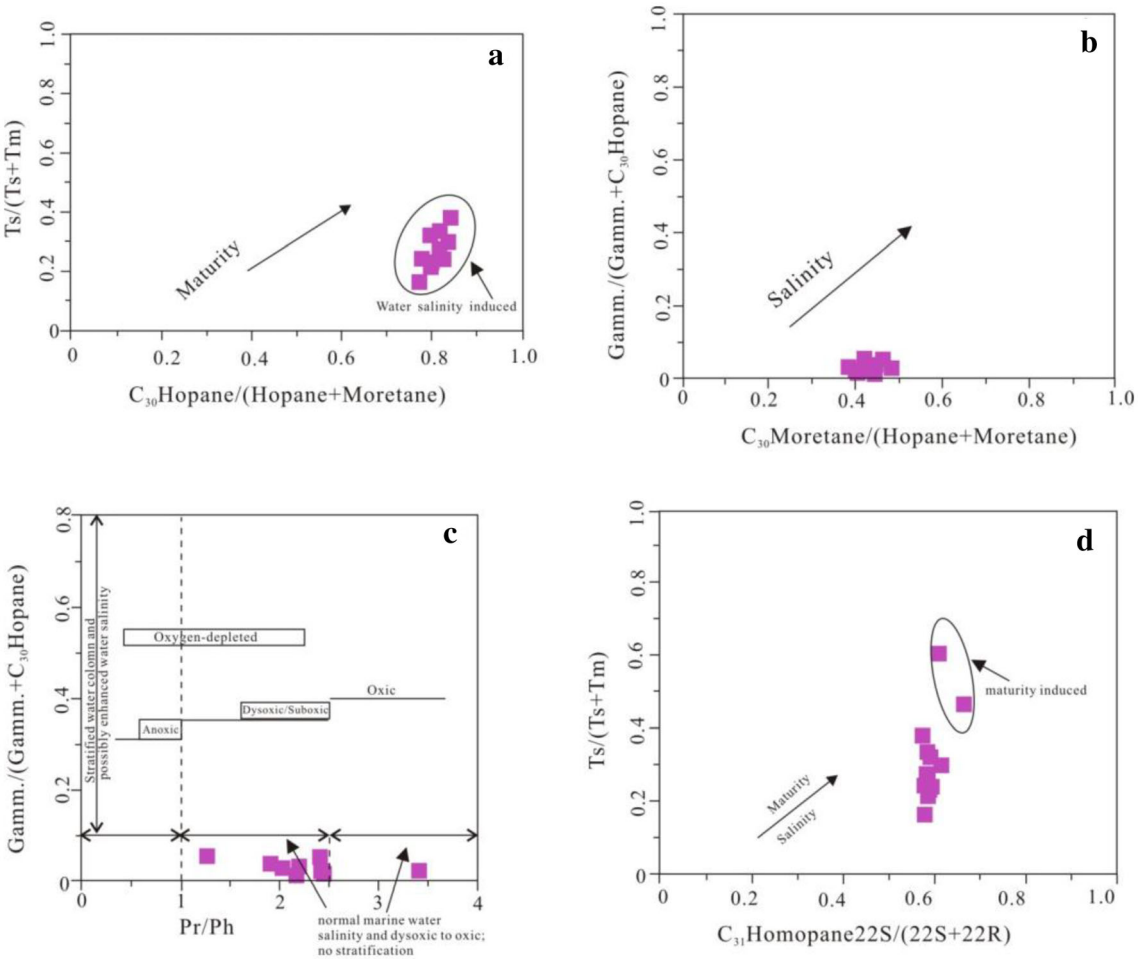

Fig. 9 Molecular indicators of Water salinity by Pr, Ph, and hopanes, and steranes. **a** Ts/(Ts + Tm) vs. C_{30} hopane/(Hopane + Moretane), **b** gammacerane index vs. C_{30} Moretane/(Hopane + Moretane), **c** gammacerane index vs. Pr/Ph and **d** Ts/(Ts + Tm) vs. 22S/(22S + 22R) C_{31} Homohopane ratios for selected samples from Amdo 114 station, Qiangtang Basin (Tibet, China)

Maturity-related biomarkers and S_1, S_2, and HI indicate that all samples in the studied area were immature or of early oil window maturity. According to organic geochemical parameters, these Middle Jurassic source rocks from the Qiangtang Basin (northern Tibet, China) are characterized by a relatively elevated abundance of organic matter, type II kerogens, and modest thermal maturity, which suggests that the Qiangtang Basin has favorable petroleum potential.

Acknowledgements We would like to thank Minquan Xia, Maocheng Wang for their fieldwork. Many thanks are also given to Mrs. Sun Weiling for the Organic geochemistry experiments at the National Research Center of Geoanalysis (Beijing, China). This study was supported by the National Natural Science Foundation of China (Grants Nos. 41572095, 42172121, 41102066, and 41572089) and the Opening Foundation of the State Key Laboratory of Marine Geology, Tongji University (China) (Grant No. MGK1703). Hugh Jenkyns (University of Oxford, UK) helped with the English language and style. We are grateful to Editor Dr. Binbin Wang and anonymous reviewers for their constructive comments and suggestions on this manuscript.

Declarations

Conflict of interest On behalf of all authors, the corresponding author states that there is no conflict of interest.

References

Aderoju T, Bend S (2018) Reconstructing the palaeoecosystem and palaeodepositional environment within the Upper Devonian-Lower Mississippian Bakken Formation: abiomarker approach. Org Geochem 119:91–100

Bechtel A, Gruber W, Sachsenhofer RF, Gratzer R, Püttmann W (2001) Organic geochemical and stable carbon isotopic investigation of coals formed in lowlying and raised mires within the Eastern Alps (Austria). Org Geochem 32:1289–1310

Behar F, Beaumont V, De B, Penteado HL (2001) Rock-Eval 6 technology: performances and developments. Oil Gas Sci. Technol. Rev. 56(2):111–134

Bingham EM, McClymont EL, Väliranta H, Mauquoy D, Roberts Z, Chambers FM, Pancost RD, Evershed RP (2010) Conservative composition of *n*-alkane biomarkers in Sphagnum species: implications for paleoclimate reconstruction in ombrotrophic peat bog. Org Geochem 41:214–220

Blumenberg M, Thiel V, Riegel W, Kah LC, Reitner J (2012) Biomarkers of black shales formed by microbial mats, late mesoproterozoic (1.1 Ga) Taoudeni Basin. Mauritania Precambrian Res 196–197:113–127

Bray EE, Evans ED (1961) Distribution of neparaffins as a clue to the recognition of source beds. Geochim Cosmochim Acta 22:2–15

Brocks JJ, Summons R (2003) Sedimentary hydrocarbons, biomarkers for early life. Treatise Geochem 8:63–115

Chen L, Yi HS, Hu RZ (2003) The discovery of Jurassic coccolithophore in Qiangtang area of northern Tibetan plateau and its significance. Earth Science Frontiers (China University of Geosciences, Beijing) 10(4):613–618 (**in Chinese with English abstract**)

Chen L, Yi HS, Zhong H, Hu RZ, Yin JR, Yang JK (2006) A calcareous nannofossils record and its geological significance in the Jurassic black shales from the Qiangtang Basin, northern Tibetan Plateau. Progress Nat Sci 16:264–273

Chen L, Xu GW, Da XJ, Ji CJ, Yi HS (2014) Biomarkers of Middle to Late Jurassic marine sediments from a canonical section: new records from the Yanshiping area, northern Tibet. Mar Pet Geol 51:256–267

Chen L, Jenkyns HC, Xu GW, Mattioli E, Da XJ, Yi HS, Xia MQ, Zhu ZX, Huang ZH (2016) Preliminary nannofossil and geochemical data from Jurassic black shales from the Qiangtang Basin, northern Tibet. J Asian Earth Sci 115:257–267

Chen L, Xu GW, Da XJ, Yi HS, Zhu ZX, Huang ZH, Li XG (2017) Chemo- and biostratigraphy of the Early Jurasic oil shales from the Qiangtang basin, northern Tibet, China: a case study for the Toarcian Oceanic Anoxic Event. Acta Geol Sin 91:630–643

Chen L, Mattioli E, Da XJ, Jenkyns HC, Zhu ZX, Xu GW, Yi HS (2019) *Calcareous nannofossils* from the Jurassic black shales in the Qiangtang Basin, Northern Tibet (China): new records of stratigraphic ages and palaeoceanography. Newsl Stratigr 52:55–72

Cheng B, Chen ZH, Chen T, Yang CY, Wang TG (2018) Biomarker signatures of the Ediacaran-Early Cambrian origin petroleum from the central Sichuan Basin, South China: implications for source rock characteristics. Mar Pet Geol 96:577–590

Didyck BM, Simoneit BRT, Brassel SC, Eglinton G (1978) Organic geochemical indicators of palaeoenvironmental conditions of sedimentation. Nature 272:216–222

Espitalié J (1993) Rock Eval pyrolysis. In: Bordenave ML (ed) Applied petroleum geochemistry. Technip, Paris, pp 237–261

Espitalié J, Deroo G, Marquis F (1986) La pyrolysis Rock-Eval et ses applications. Troisième Partie Rev Inst Fr Pétrol 41(1):73–89

Guitang P, WangLiquan LR, Sihua Y, Wenhua Ji, Fuguang Y, Wanping Z, Baodi W (2012) Tectonic evolution of the Qinghai-Tibet Plateau. J Asian Earth Sci 53:3–14

GSC (Geological Survey of China), CIGMR (Chengdu Institute of Geology and Mineral Resources) (2013) Geological map of Tibet (China) and adjacent areas (1: 1500000) with an explanation. Chengdu Cartographic Press, Chengdu

Hughes WB, Albert T, Holba G, Dzou L (1995) The ratios of dibenzothiophene to phenanthrene and pristane to phytane as indicators of depositional environment and lithology of petroleum source rocks. Geochim Cosmochim Acta 59:3581–3598

Jefferies RPS, Minton P (1965) The mode of life of two Jurassic species of "Posidonia" (Bivalvia). Palaeontology 8:156–185

Mattioli E, Erba E (1999) Biostratigraphic syntesis of calcareous nannofossil events in the Tethyan Jurassic. Riv Ital Paleontol Stratigr 105:343–376

Peters, K.E., Walters, C.C., Moldowan, J.M., 2005. The biomarker guide. biomarkers and isotopes in the environment and human history, petroleum systems and Earth History, vol I and II. Cambridge University Press, Cambridge.

Quijano ML, Castro JM, Pancost RD, de Gea GA, Najarro M, Aguado R, Rosales I, Martín-Chivelet J (2012) Organic geochemistry, stable isotopes, and facies analysis of the Early Aptian OAE-New records from Spain (Western Tethys). Palaeogeogr Palaeoclimatol Palaeoecol 365–366:276–293

Rashby SE, Sessions AL, Summons RE, Newman DK (2007) Biosynthesis of 2-methyl bacteriohopanepolyols by an anoxygenic phototroph. Proc Natl Acad Sci 104:15099–21510

Sachse VF, Littke R, Jabour H, Schümann T, Kluth O (2012) Late Cretaceous (Late Turonian, Coniacian and Santonian) petroleum source rocks as part of an OAE, Tarfaya Basin. Morocco Mar Pet Geol 29:35–49

Scalan RS, Smith JE (1970) An improved measure of the oddeeven predominance in the normal alkanes of sediment extracts and petroleum. Geochim Cosmochim Acta 34:611–620

Sinninghé-Damsté JP, Kenig F, Koopmans MP, Koster JG, Schouten S, Hayes JM, De Leeljw JW (1995) Evidence for gammacerane as an indicator of water column stratification. Geochim Cosmochim Acta 59:1895–1900

Song JL, Littke R, Weniger P (2017) Organic geochemistry of the Lower Toarcian Posidonia Shale in NW Europe. Org Geochem 106:76–92

Summons RE, Jahnke LL, Hope JM, Logan GA (1999) 2eMethylhopanoids as biomarkers for cyanobacterial oxygenic photosynthesis. Nature 400:554–557

ten Haven HL, de Leeuw JW, Rullkotter J, Sinninghe-Damsté J (1987) Restricted utility of the pristane/phytane ratio as a palaeoenvironmental indicator. Nature 330:641–643

Waples DW, Machihara T (1991) Biomarkers for geologists-A practical guide to the appilication of steranes and triterpanes in petroleum geology. AAPG Methods Explor 9:19–40

Wu ZH, Liu ZW, Zhao Z, Ji CJ, Ye PS (2016) Thrust and uplift of the Lung'erni-Angdarco paleo-oil reservoirs in the Qiangtang basin. Acta Geological Sinica 90(4):615–627 ((**in Chinese with English Abstract**))

Xu HY, George SC, Hou DJ (2019) The occurrence of isorenieratane and 24-*n*-propylcholestanes in Paleogene lacustrine source rocks from the Dongying Depression, Bohai Bay Basin: implications for bacterial sulfate reduction, photic zone euxinia and seawater incursions. Org Geochem 127:59–80

Zhang KJ, Zhang YX, Tang XC, Xia B (2012) Late Mesozoic tectonic evolution and growth of the Tibetan plateau prior to the Indo-Asian collision. Earth Sci Rev 114:236–249

Zhang YX, Li ZW, Yang WG, Zhu LD, Jin X, Zhou XY, Tao G, Zhang KJ (2017) Late Jurassic-Early Cretaceous episodic development of the Bangong Meso-Tethyan subduction: Evidence from elemental and Sr–Nd isotopic geochemistry of arc magmatic rocks, Gaize region, central Tibet, China. J Asian Earth Sci 135:212–242

Zhu DC, Li SM, Cawood PA, Wang Q, Zhao ZD, Liu SA, Wang LQ (2016) Assembly of the Lhasa and Qiangtang terranes in central Tibet by divergent double subduction. Lithos 245:7–17